TABLE I Results of Corrective Osteotomy for Cubitus Varus Deformity

	Radiographic Evaluation						Clinical Evaluation*			
		Humerus-Elbow-Wrist Angle† *(deg)*			Tilting Angle† *(deg)*			Range of Elbow Flexion-Extension *(deg)*	Pain	
Case	Time to Bone Union *(mo)*	Preop.	Postop.	Normal Side	Preop.	Postop.	Normal Side	Preop.	Postop.	Preop.	Postop.
1	2	−15	5	5	−10	25	25	95/35	130/10	None	None
2	5	−20	5	6	30	32	35	140/5	140/0	None	None
3	3	−23	4	7	27	25	25	130/−25	130/−20	None	None
4	3	−21	−5	7	30	30	30	140/−10	135/−5	None	None
Avg.	3.3	−19.8	2.3	6.3	19.3	28.0	28.8	126/1	134/−4		

*No significant difference was found between preoperative and postoperative ranges of elbow motion and pain. †No significant difference was found between the postoperative radiographic parameters and those of the unaffected, normal side. Negative values for the humerus-elbow-wrist angle and the tilting angle represent varus and hyperextension deformity of the distal part of the humerus, respectively.

months (range, five to twenty-three months) for malunited distal radial fractures.

Radiographic and Clinical Evaluation

Radiographic and clinical evaluations were conducted for all patients before surgery and at the most recent follow-up evaluation. Union was considered complete when the osteotomy line had disappeared and osseous trabecular continuity was confirmed. For cubitus varus deformities, the humerus-elbow-wrist angle[26] (defined by the longitudinal humeral axis and a line passing through the proximal and distal midpoints of the radius and ulna) and the tilting angle[27,28] (the anterior tilt of the articular condyles with respect to the long axis of the humerus) were examined with anteroposterior and lateral radiographs of the upper extremity made with the forearm in a supinated position. For malunited forearm fractures, anteroposterior and lateral radiographs made with the forearm in neutral position or in full supination were compared with

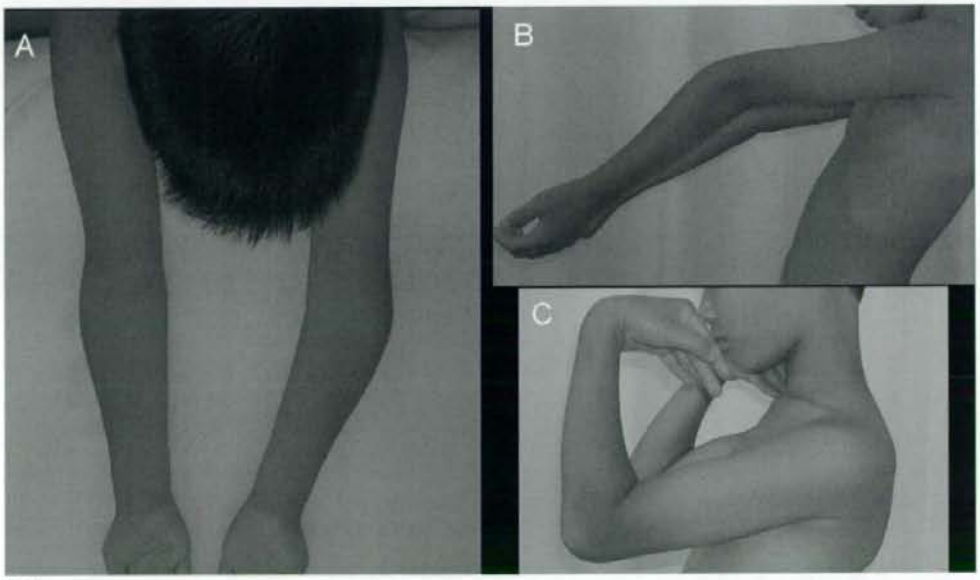

Fig. 7

Case 1. A ten-year-old boy presented with a left cubitus varus deformity (A) accompanied by hyperextension of the elbow (B) and restriction of elbow flexion to 95°(C).

Fig. 8

Case 1. Preoperative anteroposterior (A) and lateral (B) radiographs show the varus and hyperextension deformity of the distal end of the humerus.

those of the contralateral, normal side. The angular deformities of the radius and/or ulna were measured in reference to the contralateral forearm with use of the radiographs made with the forearm in the same position[29]. The greater angle of deformity between the anteroposterior and lateral radiographs was defined as the radiographic deformity angle. For malunited distal radial fractures, volar tilt, radial inclination, and ulnar variance were evaluated from wrist radiographs[30]. The values used in our study were the average of those of two independent reviewers (K.O. and H.M.). For clinical evaluation, ranges of motion of the adjacent joint were measured. Forearm rotation was measured with use of a goniometer with the humerus in a vertical position and the elbow in 90° of flexion[31]. Wrist flexion-extension was measured with the goniometer placed along the axis of rotation of the respective joints and with the forearm in a neutral position[9,32]. Grip strength was measured with use of a Jamar dynamometer (Matsumiya Medical Instruments, Tokyo, Japan) and was recorded as a percentage of that of the contralateral, normal side. Pain at the adjacent joint was graded as none (no pain), mild (occasional pain with excessive use of the hand), moderate (persistent, but endurable, pain), or severe pain necessitating analgesic control. The level of satisfaction was graded by the patient as very satisfied, satisfied, neither satisfied nor dissatisfied, dissatisfied, or very dissatisfied[33].

Statistical Methods

The differences between the radiographic values of the extremity that had been operated upon and the values from the normal side, and the differences between the preoperative and postoperative range of motion and grip strength for each deformity group, were determined by paired t test. Preoperative and postoperative scores for pain in each deformity group were compared with use of the Wilcoxon signed-rank test. Significance was established at $p < 0.05$.

Results

Cubitus Varus Deformity (Table I)

All osteotomy sites had united by an average of 3.3 months (range, nine to twenty-two weeks) after surgery. The average humerus-elbow-wrist angle and tilting angle were 20° (varus alignment) and 19°, respectively, before surgery and 2° (valgus alignment) and 28° after surgery. In one cubitus varus deformity (Case 4), although the deformity was completely corrected and fixed with Kirschner wires and suture wires, reduction was lost in the early postoperative course. The patient did not want additional surgery, and the osteotomy site united with moderate displacement. The humerus-elbow-wrist angle in this patient had been 21° (varus alignment) before surgery, 7° (valgus alignment) just after surgery, and 5° (varus alignment) at the most recent follow-up evaluation.

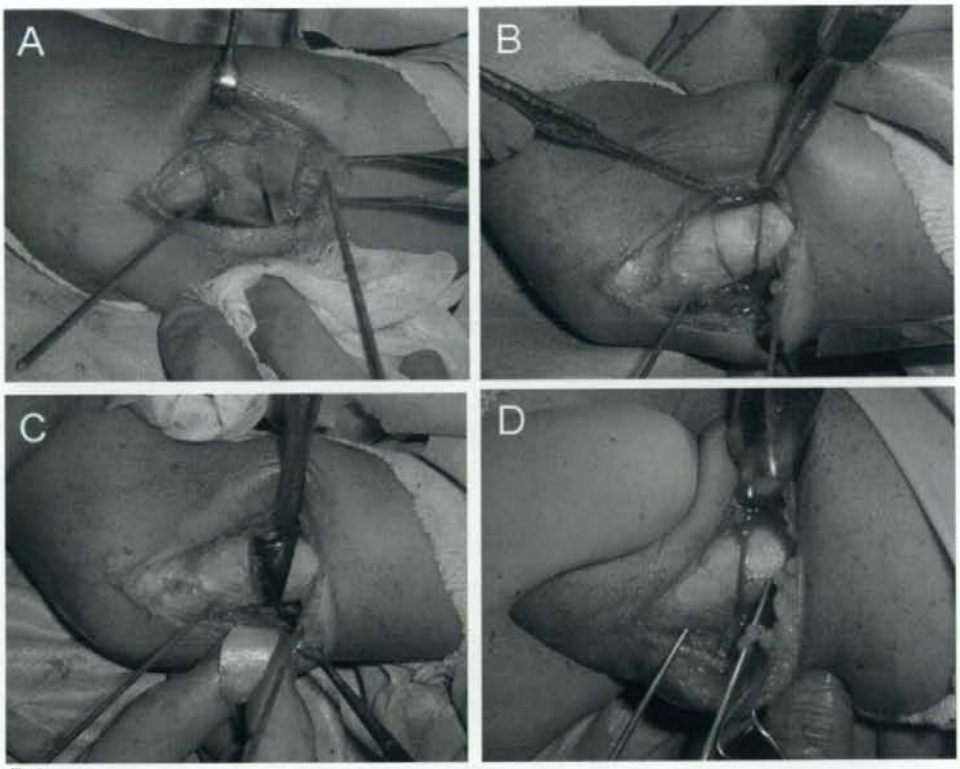

Fig. 9

The osteotomy template has been placed on the dorsolateral surface of the humerus through a lateral approach and fixed with Kirschner wires (A). The osteotomy has been accomplished through the slits on the template, which was then removed (B and C), and the osteotomy site was closed (D).

Except for this patient, the average humerus-elbow-wrist angle improved from 19° (varus alignment) before surgery to 5° (valgus alignment) after surgery. One patient with a cubitus varus deformity (Case 1) who had elbow hyperextension and restricted flexion attained normal range of elbow motion after surgery (Figs. 7 through 11). The range of elbow joint motion of the other patients with cubitus varus did not change significantly. Three patients were very satisfied with the operation, and one patient (Case 4) was neither satisfied nor dissatisfied with the operation. One patient (Case 2) complained of mild discomfort around the hardware, which was subsequently removed.

Malunited Forearm Fracture (Table II)

The osteotomy sites united an average of sixteen weeks (range, eight to twenty-six weeks) after surgery. The average angle of deformity before surgery was 16° (range, 5° to 33°) compared with the normal side. It was well corrected to 1° (range, 0° to 3°) after surgery. No distal radioulnar joint discrepancy was observed on the radiographs of the involved forearm compared with the normal side. The average range of forearm pronation and supination significantly improved from 60° and 19°, respectively, before the operation to 82° and 73° after the operation ($p < 0.01$ for both). Restricted forearm supination persisted in one patient (Case 5) with malunited fractures of both bones of the forearm, although the malunions were well corrected. In this patient, the initial injury had occurred when the patient was seven years old, and corrective surgery was performed when she was sixteen years old. It was believed that changes in joint configurations and soft-tissue contractures during this long period of time were the cause of the residual restricted forearm supination. Five patients reported pain in the adjacent joint before surgery; four of them (Cases 6, 11, 12, and 14) experienced pain in the distal radioulnar joint and one (Case 7) had pain in the proximal radioulnar joint. The preoperative pain experienced by all of these patients disappeared or decreased substantially after surgery. Painful recurrent dislocation of the radial head in one patient (Case 7), with mal-

Fig. 10

Appropriate correction was obtained as evident on the anteroposterior (A) and lateral (B) radiographs made after the closing wedge osteotomy.

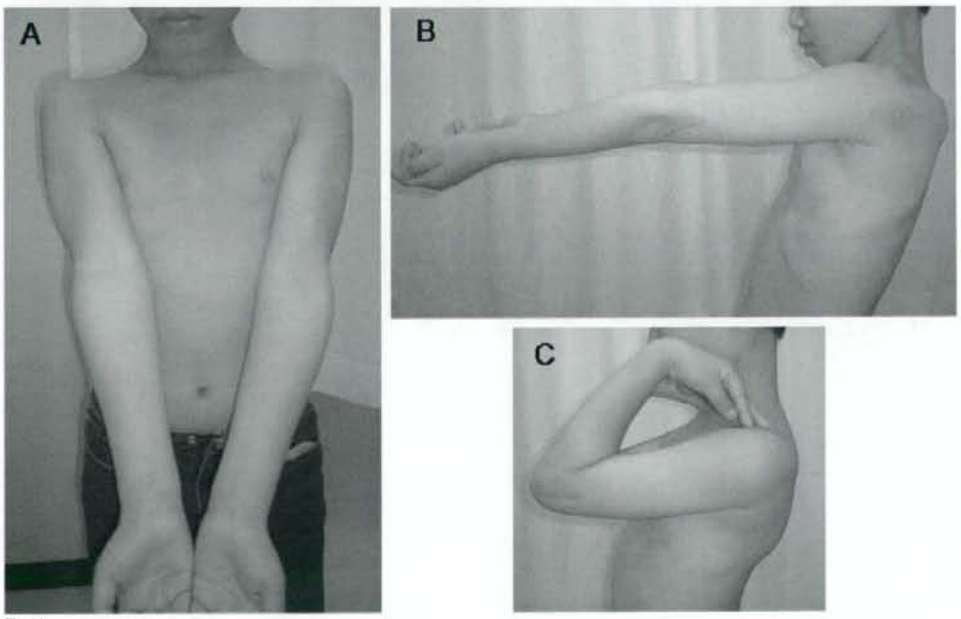

Fig. 11

The varus deformity has been corrected (A), and hyperextension and flexion of the elbow improved after surgery (B and C).

TABLE II Results of Corrective Osteotomy for Malunited Forearm Fractures

	Radiographic Evaluation				Clinical Evaluation				
			Deformity Angle* *(deg)*		Range of Forearm† (Pronation/Supination) *(deg)*			Pain†	
Case	Malunited Bone	Time to Bone Union *(mo)*	Preop.	Postop.	Preop.	Postop.	Normal Side	Preop.	Postop.
5	Radius	6	12	0	80/−30	80/10	80/90	None	None
	Ulna	6	5	0					
6	Radius	4	10	3	50/45	60/70	90/90	Moderate	Mild
	Ulna	4	5	0					
7	Radius	3	18	0	90/90	90/90	90/90	Moderate	None
	Ulna	4	16	2					
8	Radius	5	33	0	10/15	95/80	80/95	None	None
	Ulna	4	15	3					
9	Radius	3	22	0	60/−20	70/70	80/90	None	None
10	Radius	3	25	0	80/30	90/90	90/90	None	None
11	Radius	4	15	0	90/0	85/75	85/90	Mild	None
12	Radius	3	21	2	50/−15	80/70	90/70	Moderate	Mild
13	Ulna	2	30	0	10/60	80/90	80/90	None	None
14	Radius	4	6	0	80/10	90/80	90/90	Moderate	None
	Ulna	3	13	0					
Avg.		3.8	16.4	0.7	60/19	82/73	86/89		

*The deformity angle was the angle of radiographic angular deformity measured in reference to the contralateral, normal bone in the same position (see Radiographic and Clinical Evaluation section). †A significant difference was found between the preoperative and postoperative values ($p < 0.01$). ‡No significant difference was found between the preoperative and postoperative level of pain.

united fractures of both bones of the forearm, disappeared after corrective osteotomy without soft-tissue reconstruction, and the patient was able to resume sports activity. Six patients were very satisfied, and four patients were satisfied with the surgery.

Malunited Distal Radial Fracture (Table III)

All osteotomy sites had united an average of ten weeks (range, eight to thirteen weeks) after surgery. The mean volar tilt, radial inclination, and ulnar variance were −17°, 14°, and 3.4 mm, respectively, before the operation and 8°, 23°, and 0.6 mm at the final follow-up evaluation. The average wrist flexion and extension improved from 33° and 54°, respectively, before surgery to 62° and 66° after surgery ($p < 0.01$ for both). The average ranges of forearm pronation and supination improved from 58° and 69°, respectively, before surgery to 79° and 78° after surgery ($p = 0.042$). Restricted forearm supination persisted in one patient (Case 20), although the malunion was well corrected. In this patient, we believe that preexisting distal radioulnar subluxation that was not addressed well during surgery was the cause of the residual forearm rotation loss. The average grip strength improved from 42% to 86% of that of the normal side. All eight patients experienced wrist pain before surgery, which disappeared or decreased after surgery ($p = 0.013$). Three patients (Cases 16, 21, and 22) complained of discomfort around the hardware, which was subsequently removed. Four patients were very satisfied, three were satisfied, and the remaining patient (Case 20) was neither satisfied nor dissatisfied with the operation.

Complications

Postoperative partial loss of correction occurred in one patient with cubitus varus deformity. One patient who underwent surgery for cubitus varus deformity and three patients who underwent surgery for a malunited distal radial fracture complained of hardware-related pain or discomfort that necessitated hardware removal. Distal radioulnar subluxation in one patient with a malunited distal radial fracture persisted after surgery. No other major complications, including nonunion, neurovascular compromise, or infection, were observed.

Discussion

Malunion of the forearm bones, cubitus varus deformity, and a malunited distal radial fracture are typical posttraumatic deformities of the upper extremity. Symptoms and functional impairments related to these deformities may cause serious disabilities[26,30,31,34-36]. Although corrective osteotomies have been performed to improve the function and appearance

TABLE III Results of Corrective Osteotomy for Malunited Distal Radial Fractures

	Radiographic Evaluation								
	Time to Bone Union	Volar Tilt*† (deg)			Radial Inclination* (deg)			Ulnar Variance* (mm)		
Case	(mo)	Preop.	Postop.	Normal Side	Preop.	Postop.	Normal Side	Preop.	Postop.	Normal Side
15	3	−20	10	10	13	25	26	4	2	1.5
16	2	−10	9	10	−2	20	23	2	0	0
17	2	−25	5	7	15	27	28	3	0	0
18	2	−22	5	5	20	23	24	3	1.5	1
19	2	−10	5	5	10	22	23	3	0	0
20	3	−15	8	7	16	25	24	2	0	0
21	3	0	8	8	21	23	23	3	1	0
22	2	−35	10	10	15	19	20	7	0	0
Avg.	2.4	17	8	8	14	23	24	3.4	0.6	0.3

*No significant difference was found between the postoperative radiographic parameters and those of the unaffected, normal side. †A negative value for volar tilt represents extension of the articular surface. ‡A significant difference was found between the preoperative and postoperative values ($p < 0.05$). §A significant difference was found between the preoperative and postoperative values ($p < 0.01$).

of the extremity, it is not easy to correct three-dimensionally complex osseous deformities accurately[2-4,7,8,16,31,37]. Previous studies have suggested the usefulness of frontal and sagittal radiographs in the preoperative planning of a corrective osteotomy, although estimation of three-dimensional deformities with two-dimensional images has limitations[5,6,9,12,38,39]. Failure to make an accurate correction may lead to inferior clinical results, especially in the upper extremity, where anatomical bone configuration is of considerable importance to function[1-5,8,9,31,35,38,39]. To solve these problems, we developed a novel computer-assisted system to guide corrective osteotomy[15-17]. Our program can indicate the optimum pattern and plane of corrective osteotomy by calculating the axis and amount of three-dimensional deformity. The osteotomy template navigates the surgical procedure to realize the preoperative simulation.

Restricted forearm rotation is the key problem associated with malunions of the forearm bones[4,35,36,39]. Correct rotational alignment, restoration of normal length, and achievement of axial alignment of both bones are necessary to obtain a good range of forearm rotation[40]. Cadaver and clinical studies have suggested that angular deformity of the radius and/or ulna of >10° causes limitations of forearm rotation[3,4,31,39], although the relation between the severity of the deformity and the decrease in forearm rotation has not been clearly established. Contracture of the interosseous membrane, the distal and proximal radioulnar joint capsules, and other surrounding soft tissues is an additional cause of restricted forearm rotation. In long-standing forearm deformity, a combination of these factors is probably responsible for the substantial pathology of restricted range of forearm rotation[36]. In corrective surgery, the challenge is to reduce two parallel rotating long bones while maintaining the congruity of the adjacent joints[35]. Trousdale and Linscheid[36] reported the clinical results of corrective osteotomy of forearm malunion. The average arc of forearm rotation improved to only 102° in chronic forearm malunions treated more than twelve months after the initial injury, whereas it improved to 156° in those treated within twelve months of the initial injury. They concluded that corrective osteotomy for a posttraumatic malunion was best performed within twelve months of the initial fracture. They did not refer to any radiographic parameters. In our series, the average forearm rotation in the patients managed late and in those managed early improved to 152° and 159°, respectively, and angular deformities were well corrected in both groups. Although restricted forearm supination remained in one patient (Case 5), who had undergone surgery nine years after the initial injury, the range of forearm rotation had improved by 40° at the time of the final follow-up. These results indicate that an accurate three-dimensional correction of a deformity of the forearm bones can yield reasonable improvement in forearm motion, even when performed long after the initial injury.

Cubitus varus deformity is a malunion of the distal end of the humerus that generally includes varus, internal rotation, and hyperextension deformities[8,9,28,41]. In the past, it was considered a cosmetic problem, and correction of varus deformity alone has been an accepted practice[26,42,43]. Recently, because joint laxity[34,44] and tardy ulnar nerve palsy[45,46] have been reported as late complications, several investigators have advocated that correction of frontal plate angular deformity is not enough and that rotational deformity should also be corrected[8,9,41]. In fact, internal rotation of the distal end of the humerus of >25° exists in 22% of patients with a cubitus varus deformity[47]. In our opinion, this should not be overlooked,

TABLE III (*continued*)

Clinical Evaluation									
Range of Forearm Motion† (Pronation/Supination) *(deg)*			Range of Wrist Motion§ (Flexion/Extension) *(deg)*			Grip Strength§ *(% of Normal Side)*		Pain†	
Preop.	Postop.	Normal Side	Preop.	Postop.	Normal Side	Preop.	Postop.	Preop.	Postop.
60/90	80/90	80/90	30/55	70/75	80/70	13	83	Moderate	None
60/45	90/90	90/90	30/35	60/70	70/70	22	82	Moderate	Mild
60/90	75/80	90/90	20/60	65/65	70/70	75	95	Moderate	None
10/90	90/90	90/90	25/70	70/70	70/70	48	95	Moderate	None
65/70	90/90	90/90	40/65	70/85	75/85	50	97	Moderate	None
80/10	70/10	90/90	50/30	40/20	70/70	–	–	Mild	Mild
60/80	60/90	90/90	50/60	50/65	70/70	63	75	Moderate	None
70/80	80/80	80/80	20/60	75/80	80/80	26	76	Moderate	None
58/69	79/78	88/89	33/54	62/66	73/73	42	86		

considering its effect on shoulder motion and the appearance of the extremity[48]. Previously reported attempts at three-dimensional correction, however, were based on preoperative planning with use of data from plain radiographs and changes in the range of shoulder motion[9,28,43]. This procedure was also criticized for its technical difficulty and the poor osseous contact achieved at the osteotomy site[26]. In contrast, our system provides a simple and accurate correction based on three-dimensional data. The contact area at the osteotomy site can be visualized easily with use of three-dimensional images, which allow practical planning. The results of the present study, in which the postoperative humerus-elbow-wrist angle was an average of 5° and was within 3° of that of the contralateral, normal side, were the same as or better than those of previous studies[8,41,42]. Yamamoto et al.[28] performed a three-dimensional corrective osteotomy in seven patients, and a hyperextension deformity ranging from 5° to 20° persisted after surgery in three patients. In our series, the tilting angle improved to 28°, on the average, and was almost the same as that of the contralateral, normal side in all patients, including one patient (Case 1) who had 35° of hyperextension deformity before surgery.

Malunion of the distal end of the radius is one of the most common deformities of the upper extremity. Dorsal tilt, radial shortening, and a decrease in radial inclination have been cited by several investigators when attempting to plan three-dimensional correction with use of plain radiographs[1,2,49-53]. Fernandez[49,50] suggested preoperative planning with use of frontal and sagittal plane radiographs and reported good clinical results, with postoperative ranges of 50° of flexion and 57° of extension at the wrist at the time of the final follow-up. However, dorsal tilt of the distal end of the radius remained in eight of the thirty-five patients, and radial shortening of >2 mm persisted in four of the thirty patients, in whom ulnar head resection was not performed. Athwal et al.[38] introduced a computed tomography-based computer-assisted three-dimensional surgical planner that calculates the corrected position of the distal end of the radius, including an evaluation of rotational deformity with use of the contralateral, normal wrist as the template. They applied an intraoperative guidance system, which linked the preoperative plan to an optical tracking device. In six patients, the radiographic parameters of radial inclination, volar tilt, and ulnar variance relative to the contralateral, normal wrist were 2°, 1°, and 0.4 mm, respectively. At the time of the final follow-up, the average ranges in wrist flexion and extension were 47° and 42°, respectively. However, an optical tracking system requires bulky equipment and computers, monitors, and a system operator to be present during the surgery. In our series, the error between the preoperative simulation and postoperative result was <1° for both radial inclination and volar tilt and 0.3 mm for ulnar variance. As for wrist range of motion, the average ranges of wrist flexion and extension at the time of the final follow-up were 62° and 66°, respectively. The radiographic and clinical results of correction for malunited distal radial fractures in the present study were comparable or superior to those of previous studies, and the small custom-made template was quite practical. We could exactly adjust the postoperative ulnar variance in computer simulation and could avoid ulnar head resection, which has often been performed with conventional osteotomies[49,50,54].

The preliminary results in our twenty-two patients indicate that this simulation technique is a clinically reliable method. Three-dimensionally complex deformities can be accurately corrected with a simple one or two-plane osteotomy. The shortcomings of our technique include radiation exposure during computed tomography scanning, the time and effort required for computer simulation, the cost of the custom-made template, and the use of software that is not available to the public. A previous experimental study showed that radiation exposure with this system can be reasonably reduced compared with typical doses of radiation from conventional

diagnostic computed tomography scanning[55]. Computer simulation takes two to three hours for a trained operator. The time and cost of manufacturing the template are three to eight hours and about US$50, respectively. The software is currently used only in our institute for this specific clinical study; however, we plan to distribute it in the near future.

Because this study is based on a preliminary series, it has several limitations such as a relatively small number of patients in each of the corrective osteotomy groups and the absence of a control group. An additional criticism is that a minor deformity after a distal radial fracture could be corrected reasonably well without use of this technique. Therefore, further investigation is needed to determine its clinical value. However, the results of this series are encouraging. We hope that the three-dimensionally accurate correction realized by our technology will contribute to the field of deformity correction of the upper extremities.

Appendix

(eA) A table showing the clinical details of all study subjects and videos demonstrating the simulation technique are available with the electronic versions of this article on our web site at jbjs.org (go to the article citation and click on "Supplementary Material"). The table is also available on our quarterly CD/DVD (call our subscription department, at 781-449-9780, to order the CD or DVD). ■

NOTE: The authors thank Takeshi Yoshida, MD, Kakuro Denno, MD, Mitsuru Horiki, MD, and Koichi Tada, MD, from the Department of Orthopaedic Surgery, Kansai Rosai Hospital; Kozo Shimada, MD, from the Department of Orthopaedic Surgery, Osaka Koseinenkin Hospital; Shunichi Hemmi, MD, from the Department of Orthopaedic Surgery, Ikeda Municipal Hospital; Yoshiharu Nakamura, MD, from the Department of Orthopaedic Surgery, Sakai Municipal Hospital; and Ryoji Nakao, computer programmer, Department of Orthopaedic Surgery, Osaka University Graduate School of Medicine, for their contributions to this study.

Tsuyoshi Murase, MD, PhD
Kunihiro Oka, MD, PhD
Hisao Moritomo, MD, PhD
Akira Goto, MD, PhD
Hideki Yoshikawa, MD, PhD
Kazuomi Sugamoto, MD, PhD
Departments of Orthopaedic Surgery (T.M., K.O., H.M., A.G., and H.Y.) and Orthopaedic Biomaterial Science (K.S.), Osaka University Graduate School of Medicine, 2-2, Yamada-oka, Suita, Osaka 565-0871, Japan. E-mail address for T. Murase: tmurase-osk@umin.ac.jp. E-mail address for K. Oka: oka-kunihiro@umin.ac.jp. E-mail address for H. Moritomo: moritomo@ort.med.osaka-u.ac.jp. E-mail address for A. Goto: goto-akira@umin.ac.jp. E-mail address for H. Yoshikawa: yhideki@ort.med.osaka-u.ac.jp. E-mail address for K. Sugamoto: sugamoto@ort.med.osaka-u.ac.jp

References

1. Fernandez DL. Malunion of the distal radius: current approach to management. Instr Course Lect. 1993;42:99-113.

2. Fernandez DL. Reconstructive procedures for malunion and traumatic arthritis. Orthop Clin North Am. 1993;24:341-63.

3. Matthews LS, Kaufer H, Garver DF, Sonstegard DA. The effect on supination-pronation of angular malalignment of fractures of both bones of the forearm. J Bone Joint Surg Am. 1982;64:14-7.

4. Sarmiento A, Ebramzadeh E, Brys D, Tarr R. Angular deformities and forearm function. J Orthop Res. 1992;10:121-33.

5. Bilic R, Zdravkovic V, Boljevic Z. Osteotomy for deformity of the radius. Computer-assisted three-dimensional modelling. J Bone Joint Surg Br. 1994;76:150-4.

6. Jupiter JB, Ruder J, Roth DA. Computer-generated bone models in the planning of osteotomy of multidirectional distal radius malunions. J Hand Surg [Am]. 1992;17:406-15.

7. Creasman C, Zaleske DJ, Ehrlich MG. Analyzing forearm fractures in children. The more subtle signs of impending problems. Clin Orthop Relat Res. 1984;188:40-53.

8. Usui M, Ishii S, Miyano S, Narita H, Kura H. Three-dimensional corrective osteotomy for treatment of cubitus varus after supracondylar fracture of the humerus in children. J Shoulder Elbow Surg. 1995;4:17-22.

9. Uchida Y, Ogata K, Sugioka Y. A new three-dimensional osteotomy for cubitus varus deformity after supracondylar fracture of the humerus in children. J Pediatr Orthop. 1991;11:327-31.

10. Brown GA, Firoozbakhsh K, DeCoster TA, Reyna JR Jr, Moneim M. Rapid prototyping: the future of trauma surgery? J Bone Joint Surg Am. 2003;85 Suppl 4:49-55.

11. Ellis RE, Tso CY, Rudan JF, Harrison MM. A surgical planning and guidance system for high tibial osteotomy. Comput Aided Surg. 1999;4:264-74.

12. Perry M, Banks P, Richards R, Friedman EP, Shaw P. The use of computer-generated three-dimensional models in orbital reconstruction. Br J Oral Maxillofac Surg. 1998;36:275-84.

13. Shimizu T, Fujioka F, Gomyo H, Isobe K, Takaoka K. Three-dimensional starch model for simulation of corrective osteotomy for a complex bone deformity: a case report. Foot Ankle Int. 2003;24:364-7.

14. Radermacher K, Portheine F, Anton M, Zimolong A, Kaspers G, Rau G, Staudte HW. Computer assisted orthopaedic surgery with image based individual templates. Clin Orthop Relat Res. 1998;354:28-38.

15. Moritomo H, Murase T, Goto A, Nakajima Y, Masumoto J, Sasama T, Yoshida T, Yachi K. [The usefulness of three dimensional computer simulation for surgical treatment of malunited fracture and nonunion of upper extremities]. J Jpn Soc Surg Hand. 2002;19:252. Japanese.

16. Murase T, Moritomo H, Goto A, Sugamoto K, Yoshikawa H. Does three-dimensional computer simulation improve results of scaphoid nonunion surgery? Clin Orthop Relat Res. 2005;434:143-50.

17. Murase T, Moritomo H, Sugamoto K, Yoshikawa H, Ogata K, Kawasaki K. [3D computer simulation for deformity correction of the limb]. Orthop Surg Traumatol. 2005;48:1055-60. Japanese.

18. Fuller DJ, McCullough CJ. Malunited fractures of the forearm in children. J Bone Joint Surg Br. 1982;64:364-7.

19. Lorensen WE, Cline HE. Marching cubes: a high resolution 3D surface construction algorithm. Comput Graph. 1987;21:163-9.

20. Audette MA, Ferrie FP, Peters TM. An algorithmic overview of surface registration techniques for medical imaging. Med Image Anal. 2000;4:201-17.

21. Beggs JS. Kinematics. Washington: Hemisphere Publishing; 1983. Displacement; p 33-51.

22. Kinzel GL, Hillberry BM, Hall AS Jr, Van Sickle DC, Harvey WM. Measurement of the total motion between two body segments. II. Description of application. J Biomech. 1972;5:283-93.

23. Spoor CW, Veldpaus FE. Rigid body motion calculated from spatial co-ordinates of markers. J Biomech. 1980;13:391-3.

24. Paley D, Herzenberg JE, Tetsworth K, McKie J, Bhave A. Deformity planning for frontal and sagittal plane corrective osteotomies. Orthop Clin North Am. 1994;25:425-65.

25. Paley D. Principles of deformity correction. Berlin: Springer; 2002. p 235-68.

26. Oppenheim WL, Clader TJ, Smith C, Bayer M. Supracondylar humeral osteotomy for traumatic childhood cubitus varus deformity. Clin Orthop Relat Res. 1984;188:34-9.

27. Morrey BF. Anatomy of the elbow joint. In: Morrey BF, editor. The elbow and its disorders. 3rd ed. Philadelphia: WB Saunders; 2000. p 18.

28. Yamamoto I, Ishii S, Usui M, Ogino T, Kaneda K. Cubitus varus deformity following supracondylar fracture of the humerus. A method for measuring rotational deformity. Clin Orthop Relat Res. 1985;201:179-85.

29. Roberts JA. Angulation of the radius in children's fractures. J Bone Joint Surg Br. 1986;68:751-4.

30. Gartland JJ Jr, Werley CW. Evaluation of healed Colles' fractures. J Bone Joint Surg Am. 1951;33:895-907.

31. Tarr RR, Garfinkel AI, Sarmiento A. The effects of angular and rotational deformities of both bones of the forearm. An in vitro study. J Bone Joint Surg Am. 1984;66:65-70.

32. Catalano LW 3rd, Cole RJ, Gelberman RH, Evanoff BA, Gilula LA, Borrelli J Jr. Displaced intra-articular fractures of the distal aspect of the radius. Long-term results in young adults after open reduction and internal fixation. J Bone Joint Surg Am. 1997;79:1290-302.

33. Lefevre-Colau MM, Babinet A, Fayad F, Fermanian J, Anract P, Roren A, Kansao J, Revel M, Poiraudeau S. Immediate mobilization compared with conventional immobilization for the impacted nonoperatively treated proximal humeral fracture. A randomized controlled trial. J Bone Joint Surg Am. 2007;89:2582-90.

34. O'Driscoll SW, Spinner RJ, McKee MD, Kibler WB, Hastings H 2nd, Morrey BF, Kato H, Takayama S, Imatani J, Toh S, Graham HK. Tardy posterolateral rotatory instability of the elbow due to cubitus varus. J Bone Joint Surg Am. 2001;83:1358-69.

35. Schemitsch EH, Richards RR. The effect of malunion on functional outcome after plate fixation of fractures of both bones of the forearm in adults. J Bone Joint Surg Am. 1992;74:1068-78.

36. Trousdale RT, Linscheid RL. Operative treatment of malunited fractures of the forearm. J Bone Joint Surg Am. 1995;77:894-902.

37. Rieger M, Gabl M, Gruber H, Jaschke WR, Mallouhi A. CT virtual reality in the preoperative workup of malunited distal radius fractures: preliminary results. Eur Radiol. 2005;15:792-7.

38. Athwal GS, Ellis RE, Small CF, Pichora DR. Computer-assisted distal radius osteotomy. J Hand Surg [Am]. 2003;28:951-8.

39. Dumont CE, Thalmann R, Macy JC. The effect of rotational malunion of the radius and the ulna on supination and pronation. J Bone Joint Surg Br. 2002;84:1070-4.

40. Chapman MW, Gordon JE, Zissimos AG. Compression-plate fixation of acute fractures of the diaphyses of the radius and ulna. J Bone Joint Surg Am. 1989;71:159-69.

41. Chung MS, Baek GH. Three-dimensional corrective osteotomy for cubitus varus in adults. J Shoulder Elbow Surg. 2003;12:472-5.

42. Bellemore MC, Barrett IR, Middleton RW, Scougall JS, Whiteway DW. Supracondylar osteotomy of the humerus for correction of cubitus varus. J Bone Joint Surg Br. 1984;66:566-72.

43. Graham B, Tredwell SJ, Beauchamp RD, Bell HM. Supracondylar osteotomy of the humerus for correction of cubitus varus. J Pediatr Orthop. 1990;10:228-31.

44. Abe M, Ishizu T, Nagaoka T, Onomura T. Recurrent posterior dislocation of the head of the radius in post-traumatic cubitus varus. J Bone Joint Surg Br. 1995;77:582-5.

45. Abe M, Ishizu T, Shirai H, Okamoto M, Onomura T. Tardy ulnar nerve palsy caused by cubitus varus deformity. J Hand Surg [Am]. 1995;20:5-9.

46. Spinner RJ, O'Driscoll SW, Davids JR, Goldner RD. Cubitus varus associated with dislocation of both the medial portion of the triceps and the ulnar nerve. J Hand Surg [Am]. 1999;24:718-26.

47. Mahaisavariya B, Laupattarakasem W. Supracondylar fracture of the humerus: malrotation versus cubitus varus deformity. Injury. 1993;24:416-8.

48. Laupattarakasem W, Mahaisavariya B, Kowsuwon W, Saengnipanthkul S. Pentalateral osteotomy for cubitus varus. Clinical experiences of a new technique. J Bone Joint Surg Br. 1989;71:667-70.

49. Fernandez DL. Correction of post-traumatic wrist deformity in adults by osteotomy, bone-grafting, and internal fixation. J Bone Joint Surg Am. 1982;64:1164-78.

50. Fernandez DL. Radial osteotomy and Bowers arthroplasty for malunited fractures of the distal end of the radius. J Bone Joint Surg Am. 1988;70:1538-51.

51. Posner MA, Ambrose L. Malunited Colles' fractures: correction with a biplanar closing wedge osteotomy. J Hand Surg [Am]. 1991;16:1017-26.

52. Shea K, Fernandez DL, Jupiter JB, Martin C Jr. Corrective osteotomy for malunited, volarly displaced fractures of the distal end of the radius. J Bone Joint Surg Am. 1997;79:1816-26.

53. Zdravkovic V, Bilic R. Computer-assisted preoperative planning (CAPP) in orthopaedic surgery. Comput Methods Programs Biomed. 1990;32:141-6.

54. Malone KJ, Magnell TD, Freeman DC, Boyer MI, Placzek JD. Surgical correction of dorsally angulated distal radius malunions with fixed angle volar plating: a case series. J Hand Surg [Am]. 2006;31:366-72.

55. Bonel HM, Jager L, Frei KA, Galliano S, Srivastav SK, Flohr T, Reiser MF, Dinkel HP. Optimization of MDCT of the wrist to achieve diagnostic image quality with minimum radiation exposure. AJR Am J Roentgenol. 2005;185:647-54.

SCIENTIFIC ARTICLE

Relationship Between the Fracture Location and the Kinematic Pattern in Scaphoid Nonunion

Hisao Moritomo, MD, PhD, Tsuyoshi Murase, MD, PhD, Kunihiro Oka, MD, PhD, Hiroyuki Tanaka, MD, PhD, Hideki Yoshikawa, MD, PhD, Kazuomi Sugamoto, MD, PhD

Purpose The purpose of this study was to obtain 3-dimensional and quantitative information regarding the pathological kinematics of the wrist with scaphoid nonunion using an *in vivo* and 3-dimensional motion analysis. We specifically tested the hypothesis that the fracture location is related to the kinematic pattern.

Methods We studied wrist kinematics during wrist flexion-extension motion and radioulnar deviation in 13 patients with scaphoid nonunion, using a markerless bone registration technique. Magnetic resonance images or computed tomography (CT) images of the wrist were acquired with the wrist in the neutral and 4 extreme positions of flexion, extension, radial deviation, and ulnar deviation. Three-dimensional animations were created of the carpal motions and interfragmentary motions between the distal and proximal fragments of the scaphoid. Based on the fracture location, accurate estimates of the relative positions and orientations of the carpal bones were analyzed.

Results There were 2 clear patterns of the interfragmentary motions of the scaphoid based on the fracture location. In the mobile type scaphoid nonunion (7 cases), the fracture was located distal to the apex of the scaphoid dorsal ridge (scaphoid apex), and the distal scaphoid was unstable relative to the proximal scaphoid. The distal fragment showed a "book-opening" motion from wrist flexion to extension. In the stable type scaphoid nonunion (6 cases), the fracture was located proximal to the scaphoid apex, and the interfragmentary motion was considerably less than with the distal type.

Conclusions Carpal instability following scaphoid nonunion appears to be related to whether the fracture line passes distal or proximal to the scaphoid apex, where the dorsal scapholunate interosseous ligament and the dorsal intercarpal ligament attach. Three-dimensional imaging should be considered when assessing scaphoid nonunions to identify the exact location of the fracture. This may allow the clinician to choose the best treatment option. *(J Hand Surg 2008;33A:1459–1468. Copyright © 2008 by the American Society for Surgery of the Hand. All rights reserved.)*

Key words Biomechanics, instability, scaphoid nonunion, 3-dimensional motion analysis, wrist.

Additional material is available online.

From the Department of Orthopaedics, Osaka University, Osaka, Japan.

The authors would like to acknowledge assistance during parts of the experimental procedures from Sayuri Arimitsu, MD, Department of Orthopaedics, Osaka University; Ryoji Nakao, computer programmer, Department of Orthopaedics, Osaka University; Kakuro Denno, MD, Department of Orthopaedics, Kansai Rosai Hospital; Kenji Miki, MD, Department of Orthopaedics, Amagasaki Chuou Hospital; and Mitsuru Horiki, MD, Department of Orthopaedics, Kansai Rosai Hospital.

Received for publication November 30, 2007; accepted in revised form May 29, 2008.

This study was supported in part by Grants-in-Aid for Scientific Research, the Ministry of Education, Science, and Culture of Japan.

No benefits in any form have been received or will be received related directly or indirectly to the subject of this article.

Corresponding author: Hisao Moritomo, MD, PhD, Department of Orthopaedics, Osaka University, 2-2 Yamadaoka, Suita-shi, Osaka, 565-0871 Japan; e-mail: moritomo@ort.med.osaka-u.ac.jp.

0363-5023/08/33A09-0001$34.00/0
doi:10.1016/j.jhsa.2008.05.035

THE SCAPHOID FUNCTIONS as a complex link between the proximal and distal carpal rows of the wrist.[1] The scaphoid plays an important role in wrist function; thus, scaphoid fracture nonunion changes wrist mechanics, which can lead to carpal instability and secondary degenerative changes. Although there have been a few reported factors that are responsible for carpal instability after scaphoid fracture, such as fracture location[2–4] and lunate morphology,[5] the exact mechanism of instability is still unknown.

The carpal displacements caused by scaphoid nonunion have been analyzed using 3-dimensional reconstruction of CT with the wrist in the neutral position. Two distinct offset patterns of the distal fragment with respect to the proximal fragment have been identified:[2–4] a volar type, in which the distal fragment overhangs palmarly relative to the proximal fragment; and a dorsal type, in which the distal fragment shifts dorsally relative to the proximal fragment. The volar types of scaphoid nonunion have been found to occur exclusively after fractures distal to the apex of the dorsal ridge of the scaphoid (scaphoid apex, Fig. 1), and the dorsal types have been associated with fractures proximal to the scaphoid apex.[3,4]

The nature and magnitude of the interfragmentary motion that is present in scaphoid nonunion and its kinematic effects on the remainder of the wrist are poorly understood. An *in vitro* kinematic study of the wrist after scaphoid waist osteotomy in cadavers[6] found that the distal scaphoid assumed a relatively flexed stance and had increased motion, while the proximal scaphoid and lunate assumed a relatively extended stance and had less motion. However, such *in vitro* experiments cannot completely reproduce the physical muscular force that is exerted across the wrist *in vivo*. These limitations could alter carpal motion kinematics. Recently, researchers have been able to measure the *in vivo* kinematics of the human joint using noninvasive techniques.[7–10] Such *in vivo* research may provide more accurate information about the kinematics of scaphoid nonunion.

A few *in vitro* studies have dealt with the biomechanical consequences of scaphoid fractures on wrist kinematics[6] and load distribution;[11] however, the findings have not been confirmed *in vivo*. Furthermore, it is unknown whether fracture location determines the kinematic effects that these fractures have on the remainder of the wrist. Thus, this study was designed to obtain 3-dimensional and quantitative data regarding the pathological kinematics of the wrist following scaphoid nonunion, using *in vivo* motion analysis. We specifically tested the hypothesis that the fracture location with respect to the scaphoid apex is related to the kinematic pattern.

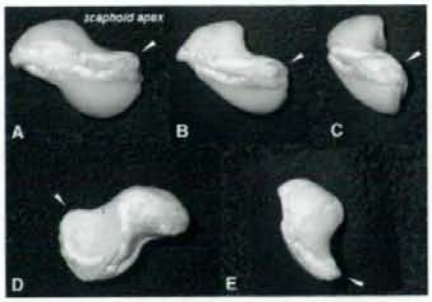

FIGURE 1: The scaphoid apex is the most dorsal and ulnar nonarticulating part of the scaphoid. The scaphoid of a right cadaver wrist seen from the **A** radial, **B** radiodorsal, **C** dorsal, **D** ulnar, and **E** distal side. The location of the *scaphoid apex* on the dorsal ridge is indicated by an arrow head.

MATERIALS AND METHODS

We studied the *in vivo* kinematics of the wrist joint during wrist flexion-extension motion and radioulnar deviation in 13 patients with scaphoid nonunion (10 men and 3 women; age range, 19–57 years; mean age, 29 years, Table 1). All patients provided their written informed consent before being enrolled in the study.

Fracture location

In order to identify the location of the scaphoid apex, we took CT scans of both wrists in the wrist neutral position for all patients, using a clinical helical type scanner (Lightspeed Ultra16, General Electric, Waukesha, WI) with a slice thickness of 0.635 mm. We determined the neutral wrist position by aligning the third metacarpal with the dorsal surface of the forearm. First, the scaphoid apex was carefully identified using the 3-dimensional image of the scaphoid, reconstructed from the CT data. The scaphoid apex is the most dorsal and ulnar nonarticulating part of the scaphoid, which is determined only by osseous geometry. The scaphoid apex can be seen from various points of view in 3-dimensional imaging (Fig. 1). Usually, to identify the scaphoid apex, the radiodorsal view is the best. Comparing it to the 3-dimensional image of the contralateral scaphoid is helpful, especially when the osteophytes exist around the fracture site. Next, the orientation of the fracture line relative to the scaphoid apex was identified on 3-dimensional imaging. The straight-line distance between the scaphoid apex and a point at which the fracture line crossed the dorsoulnar cortex of the

TABLE 1. Patient Data

Type of Scaphoid Nonunion	Case	Fracture Type: Herbert Classification	Fracture Type: Garcia-Elias Classification	Fracture Type: Our Classification	Age (Years)	Gender	Duration of Nonunion (Months)	Apex-Fracture Distance (mm)*	Radiolunate Angle (°)†	DISI Deformity	Degenerative Change
Mobile type	1	B1		Type 2	27	M	6	9.0	12	Present	Absent
	2	B1		Type 2	23	M	2	7.8	25	Present	Absent
	3	B2			20	M	33	12.9	5	Present	Absent
	4	B2			39	M	480	8.5	42	Present	Radioscaphoid joint
	5	B5			21	F	2	11.2	39	Present	Absent
	6	B3	Type 2		34	M	5	7.7	19	Present	Absent
	7	B3	Type 2		25	M	52	7.1	14	Present	Absent
	Average				**27**		**83**	**9.2**	**22**		
	SD				7		176	**2.1**	**14**		
Stable type	8	B1		Type 1	34	M	205	5.4	−10	Absent	Radioscaphoid joint
	9	B1		Type 1	19	M	9	3.1	−10	Absent	Absent
	10	B3	Type 1		26	F	11	2.4	−5	Absent	Absent
	11	B3	Type 1		26	F	48	4.5	−3	Absent	Absent
	12	B3	Type 1		57	M	7	3.7	−5	Absent	Radioscaphoid joint
	13	B3	Type 1		19	M	33	7.5	−5	Absent	Absent
	Average				**30**		**52**	**4.4**	**−6**		
	SD				**14**		**77**	**1.8**	**3**		
Total	**Average**				**28**		**69**	**7.0**	**9**		
	SD				**11**		**135**	**3.1**	**18**		

DISI, dorsal intercaleted segment instability.
*The straight line distance between the scaphoid apex and fracture line. All the fracture location in the type 2 scaphoid nonunion is distal to the scaphoid apex.
†When the lunate rotated dorsally, the radiolunate angle is shown as a minus value.

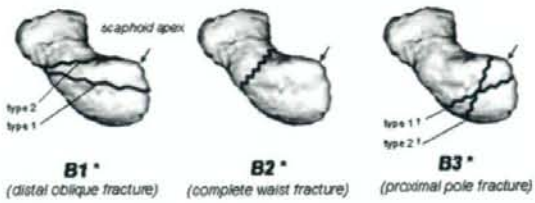

mobile type nonunion	stable type nonunion
• type 2 B1 • B2 • type 2 B3 • B5	• type 1 B1 • type 1 B3

FIGURE 2: New classification system of the scaphoid fracture based on the relationship between fracture location and the scaphoid apex. The right scaphoids are seen from the radiodorsal side. *According to Herbert's classification system of scaphoid fractures. †According to the classification system of proximal pole fractures by Garcia-Elias.

scaphoid (apex-fracture distance) was measured using specially developed software (Orthopedics Viewer, Osaka University, Osaka, Japan).

The fracture pattern was first classified based on the fracture location, using the Herbert classification system[12] (Fig. 2). There were 4 cases of B1 (distal oblique fracture), 2 cases of B2 (waist fracture), 6 cases of B3 (proximal pole fracture), and 1 case of B5 (comminuted waist fracture). The B3 cases were further classified according to the Garcia-Elias classification system.[13] Among the B3 group, there were 4 cases of type 1, where the fracture line runs proximal to the scaphoid apex, and 2 cases of type 2, where the fracture line runs distal to the scaphoid apex. We also classified the B1 cases based on the dorsal portion of the fracture relative to the scaphoid apex. Among the B1 group, there were 2 type 1 cases, where the fracture line runs proximal to the scaphoid apex, and 2 type 2 cases, where the fracture line runs distal to the scaphoid apex.

Motion analysis

In order to obtain the kinematic data (not to identify the scaphoid apex or fracture line), we used magnetic resonance imaging (4 cases) or CT (9 cases) of the wrist in 5 positions (the neutral and 4 extreme positions of flexion, extension, radial deviation, and ulnar deviation). Our kinematic analysis technique and its accuracy have been documented previously.[7] Magnetic resonance image data of the wrists were obtained using a 1.5-T commercial magnetic resonance system (Magnetom Vision PlusR 1.5-T MRI; Siemens AG, Erlangen, Germany) in conjunction with a receive-only body-array surface coil. We used a 3-dimensional sequence (3-dimensional fast low angle shot) with a repetition time of 2.3 ms, an echo time of 33 ms, a flip angle of 45°, a 160-mm field of view, and a 0.5-mm thickness, on a contiguous slice with a pixel size of 0.6 × 0.8 mm. Computed tomography images were obtained using the same technique described earlier. To immobilize the elbow and the wrist, a special positioning device was used. This device has a grip bar and has 3 motion axes that all cross perpendicularly at the wrist joint and enable the wrist to move along any specific plane. The contours of each bone were mapped from the volume images and 3-dimensional surface models of the bones were constructed. The kinematic variables were calculated by registering the bone in 1 position and then comparing the data with those of other positions. The volume registration technique[7] was used in this study. The data for all left wrists were mathematically converted into right wrist data.

The radius and all the carpal bones except the pisiform were registered, and the relative motion of each bone was calculated. The proximal and distal fragments of the scaphoid were tracked as separate carpal bones. Three-dimensional animations of carpal motion and the interfragmentary motion that occurred between the distal and proximal fragments of the scaphoid were created using originally developed software (Orthopedics Viewer, Osaka University, Osaka, Japan).

Accurate estimates of the relative positions and orientations of the bones during flexion-extension motion and radioulnar deviation were obtained using Euler angles. Euler angles describe the angular motion of a body in 3-dimensional space. In this application, the Euler angles are presented as the roll-pitch-yaw angle of the carpal bones relative to the radius. For the interfragmentary motion, the roll-pitch-yaw angle of the distal scaphoid relative to the proximal scaphoid in the wrist neutral position was used.

During wrist flexion-extension motion and radioulnar deviation, the contribution rates of the motion between the radius and distal scaphoid, the motion between the radius and proximal scaphoid, and the radiolunate motion to global wrist motion were studied. Two data points of the extreme positions for each motion plane were obtained. The radiocapitate motion was used as a global wrist motion.[8] The contribution

data in this study were compared with a database of normal wrists obtained in the previous study.[7]

The coordinate system was constructed according to the International Society of Biomechanics (http://www.isbweb.org/standards/wrist.html) definition: the origin is located midway between the distal radius at the level of the ridge between the radioscaphoid fossa and the radiolunate fossa. The Z axis is the axis of flexion and extension; the Y axis is the axis of pronation and supination; and the X axis is the axis of radial and ulnar deviation. The Y axis is the line parallel to the long shaft of the radius that intersects with the origin. The Z axis is the line perpendicular to the Y axis and in a plane defined by the tip of the radial styloid, the base of the concavity of the sigmoid notch, and the specified origin. The X axis is defined as the common line perpendicular to both the Y and Z axes.

All data are expressed as means ± SD. Statistical analysis of differences was performed using Student's *t*-test; $p<.05$ was considered significant.

RESULTS

Two clearly separate patterns of interfragmentary motions of the scaphoid and other carpal motions were identified: the *mobile* type scaphoid nonunion (7 cases) and the *stable* type scaphoid nonunion (6 cases) (Table 1). In the mobile type, the dorsal portion of the fracture was always distal to the scaphoid apex. The fracture types in this group were B1 type 2, B2, B3 type 2, and B5 (Fig. 2). The average apex-fracture distance was 9 mm (range, 7–13 mm). In the stable type, the dorsal portion of the fracture was always proximal to the scaphoid apex. The fracture types in this group were B1 type 1 and B3 type 1 (Fig. 2). The average apex-fracture distance was 4 mm (range, 2–8 mm). In the wrist neutral position, all patients with a mobile type scaphoid nonunion had an extended stance of the lunate or a dorsal intercalated segment instability (DISI) deformity, in which the radiographic radiolunate angle was 22° ± 14°. The radiolunate angle was −6° ± 3° in the stable type nonunion; none of the patients with stable type nonunion had a DISI deformity (Table 1).

Motion of the mobile type scaphoid nonunion

In the animation of wrist flexion-extension motion during which the proximal scaphoid was fixed and the other bones were moving, the distal fragment showed a "book-closing" motion during wrist flexion (the distal scaphoid rotates palmarly, and there is some overlap of the proximal and distal scaphoid segments in the sagittal view) and a "book-opening" motion during wrist extension (the distal scaphoid extends, resulting in a palmarly opening bone defect) (Fig. 3A). The distal scaphoid flexed 7° ± 10° and extended 24° ± 15° relative to the proximal scaphoid during motion from the neutral position to wrist flexion and from the neutral position to wrist extension, respectively (Table 2). The scaphoid nonunions categorized as B1 type 2 (oblique fracture, cases 1 and 2) and B3 type 2 (proximal pole fracture, cases 6 and 7, Fig. 4) were unstable during the flexion-extension motion and behaved identically to B2 (waist fracture, cases 3 and 4). The interfragmentary rotations in radioulnar deviation were much smaller than in flexion-extension motion, where the distal scaphoid flexed 0° ± 4° and extended 0° ± 12°relative to the proximal scaphoid with wrist radial deviation and ulnar deviation, respectively (Table 2). In the animation, however, the distal scaphoid appeared to impinge with the radial styloid in wrist radial deviation in all cases (Fig. 3B).

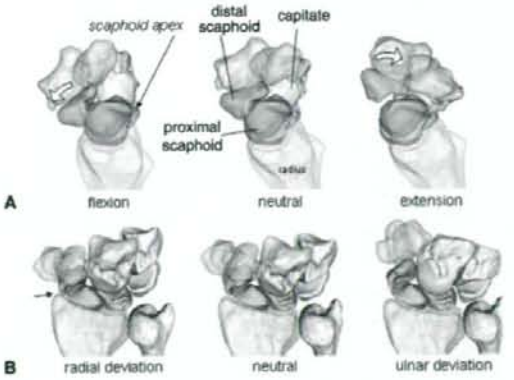

FIGURE 3: Motions of the mobile type waist nonunion (B2, case 4). **A** Radial views during wrist flexion–extension motion. The distal fragment shows a "book-closing" motion during wrist flexion and a "book-opening" motion during wrist extension. **B** Dorsal views during radioulnar deviation. Note the impingement between the distal scaphoid and the radial styloid in radial deviation (arrow). The proximal scaphoid is fixed, and the other bones are moving. (Videos can be viewed on the *Journal's* Web site, www.jhandsurg.org.)

The rotation contribution rates of the motion between the radius and distal scaphoid, the motion between the radius and proximal scaphoid, and the radiolunate motion to global wrist motion were 87%, 54%, and 39% during wrist flexion-extension, and 32%, 31%, and 1% during wrist radioulnar deviation, respectively (Table 3). The rotation contribution rates of the scaphoid and the lunate from a database of normal wrists were 82% and 56% during wrist flexion-extension, and 36%, and 37% during wrist radioulnar deviation, re-

TABLE 2. Euler Angles of Carpal Motion

Global Wrist Motion	Flexion (°)			Extension (°)			Radial Deviation (°)			Ulnar Deviation (°)		
Bone	Z	Y	X	Z	Y	X	Z	Y	X	Z	Y	X
Mobile type												
Distal scaphoid to proximal scaphoid	7 ± 10	−2 ± 2	4 ± 4	−24 ± 15	−3 ± 4	−3 ± 5	0 ± 4	−1 ± 4	1 ± 3	0 ± 12	1 ± 3	1 ± 5
Distal scaphoid to radius	40 ± 9	0 ± 5	3 ± 8	−37 ± 15	0 ± 6	0 ± 7	2 ± 10	−3 ± 5	−4 ± 7	−5 ± 17	4 ± 3	9 ± 4
Proximal scaphoid to radius	33 ± 11	2 ± 5	−1 ± 6	−13 ± 9	3 ± 4	3 ± 4	2 ± 8	−1 ± 4	−5 ± 5	−5 ± 9	3 ± 4	9 ± 5
Lunate to radius	26 ± 12	1 ± 4	−2 ± 6	−9 ± 5	1 ± 2	2 ± 6	6 ± 7	0 ± 3	−7 ± 9	−6 ± 11	1 ± 3	10 ± 7
Capitate to radius	46 ± 12	3 ± 4	1 ± 12	−43 ± 19	3 ± 5	2 ± 9	−3 ± 12	−3 ± 7	−14 ± 11	10 ± 17	−2 ± 8	29 ± 13
Stable type												
Distal scaphoid to proximal scaphoid	1 ± 8	0 ± 6	1 ± 5	−7 ± 5	−1 ± 3	0 ± 1	5 ± 5	1 ± 3	−2 ± 4	3 ± 7	1 ± 5	1 ± 4
Distal scaphoid to radius	34 ± 10	2 ± 5	3 ± 6	−23 ± 9	−6 ± 6	2 ± 2	12 ± 8	−1 ± 5	−4 ± 5	−2 ± 12	0 ± 1	13 ± 7
Proximal scaphoid to radius	33 ± 10	2 ± 4	2 ± 6	−18 ± 12	−5 ± 5	2 ± 2	8 ± 6	−2 ± 5	−3 ± 4	−5 ± 6	0 ± 5	11 ± 6
Lunate to radius	23 ± 8	2 ± 6	3 ± 6	−10 ± 7	−4 ± 4	1 ± 5	10 ± 6	−1 ± 4	0 ± 5	−5 ± 9	0 ± 1	12 ± 5
Capitate to radius	42 ± 18	2 ± 4	4 ± 12	−33 ± 16	−7 ± 9	2 ± 10	9 ± 15	−5 ± 5	−18 ± 9	12 ± 11	−1 ± 5	24 ± 10

Z, + flexion, − extension; Y, + pronation, − supination; X, + ulnar deviation, − radial deviation

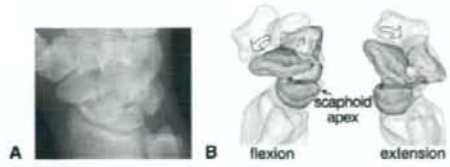

FIGURE 4: The mobile type proximal pole nonunion (B3 type 2, case 7). **A** The semipronated view of the plain radiograph does not show clear relationship between the fracture line and the scaphoid apex. **B** Three-dimensional animation shows a marked interfragmentary motion during flexion–extension motion. The proximal scaphoid is fixed, and the other bones are moving (these videos can be viewed at the *Journal's* Web site, www.jhandsurg.org).

spectively (as previously published[7]). There was a relative decrease in contribution rates of the motion between the radius and proximal scaphoid ($p<.001$) and the radiolunate motion ($p<.001$) during wrist flexion-extension and of the radiolunate motion during wrist radioulnar deviation ($p<.001$) when compared to the normal wrist.

Motion of the stable type scaphoid nonunion

The interfragmentary motion with the stable type scaphoid nonunion during wrist flexion-extension motion was significantly smaller than that with the mobile type ($p<.05$, Fig. 5A), in which the distal scaphoid flexed $1° \pm 8°$ and extended $7° \pm 5°$relative to the proximal scaphoid in wrist flexion and extension, respectively (Table 2). The interfragmentary motions in radioulnar deviation were also small (Fig. 5B), but there was not a significant difference with the mobile type. The distal scaphoid flexed $5° \pm 5°$ and extended $3° \pm 7°$ relative to the proximal scaphoid in wrist radial deviation and ulnar deviation, respectively (Table 2).

The rotation contribution rates of the motion between the radius and distal scaphoid, the motion between the radius and proximal scaphoid, and the radiolunate motion to global wrist motion were 79%, 68%, and 44% during wrist flexion-extension and 42%, 34%, and 30% during wrist radioulnar deviation, respectively (Table 3). There was a relative decrease in contribution rates of the motion between the radius and proximal scaphoid ($p<.005$) and the radiolunate motion ($p<.01$) during wrist flexion-extension when compared to normal wrists (82% and 56%, respectively).[7] There were no significant differences in contribution rates during wrist radioulnar deviation. When compared to the mobile type, there was a relative decrease in contribution rates of the motion between the radius and the distal scaphoid during wrist flexion-extension ($p<.05$) and a relative increase in contribution rates of the radiolunate motion during wrist radioulnar deviation ($p<.005$).

There was no significant relationship between the interfragmentary motion and the duration (number of months) of the nonunion or between the interfragmentary motion and degenerative changes in the mobile type and the stable type.

DISCUSSION

A few *in vitro* studies[6,11] have investigated the biomechanical consequences of scaphoid fractures; however, the findings have never been confirmed *in vivo*. Furthermore, the relationship between the fracture location and the nature and magnitude of the interfragmentary motion of the scaphoid and its kinematic effects on the reminder of the wrist are still unknown. Therefore, we designed this study to investigate the pathological kinematics of the wrist with scaphoid nonunion in terms of the fracture location using *in vivo* 3-dimensional motion analysis.

The kinematic technique used in this study has some limitations. The primary disadvantage is that this study is based on static 3-dimensional views of the carpus in a limited number of wrist positions. Static measurement does not include any inertial or functional effects that might occur during normal wrist motion. This study was conducted with only 13 patients, which results in a low power analysis. For the motion analysis, we used magnetic resonance images in 4 cases and CT in 9 cases. Although accuracy of motion analysis using magnetic resonance images has been proved previously, uniform protocol would have been more valuable. However, CT data were used in all patients regarding fracture location, and this kinematic technique allows 3-dimensional data to be collected *in vivo* and pathological kinematics to be studied noninvasively.

In previous studies dealing with 3-dimensional deformity of scaphoid nonunion at the wrist neutral position,[3,4] it was found that a humpback deformity of the scaphoid and a DISI deformity predominantly occurred following fractures in which the dorsal portions were located distal to the scaphoid apex; the deformities were less commonly associated with fractures located proximal to the apex. It was suggested that fractures distal to the insertion of the proximal fiber of the dorsal intercarpal ligament and the dorsal scapholunate interosseous ligament are destabilized and that this allows the distal fragment to flex and the proximal fragment to extend. Conversely, in proximally located fractures, the ligamentous restraints are still attached to the distal fragment

TABLE 3. Rotation Contribution Rates of the Scaphoid and Lunate Motions Respective to the Radius to Global Wrist Motion

	Mobile Type				Stable Type				Normal[6]	
	Case	Distal Scaphoid (%)	Proximal Scaphoid (%)	Lunate (%)	Case	Distal Scaphoid (%)	Proximal Scaphoid (%)	Lunate (%)	Scaphoid (%)	Lunate (%)
Flexion–extension motion	1	89	43	32	8	79	69	50		
	2	88	60	49	9	83	57	47		
	3	94	77	44	10	79	77	51		
	4	87	23	29	11	72	83	38		
	5	73	62	49	12	92	54	38		
	6	93	69	40	13	68	69	42		
	7	81	43	31						
Average		87	54	39		79	68	44	81.7	56.4
SD		7	19	9		8	11	6		
Radioulnar deviation	1	27	28	−1	8	68	66	54		
	2	51	49	2	9	29	18	27		
	3	44	45	0	10	38	41	43		
	4	21	13	8	11	47	40	45		
	5	21	14	7	12	33	11	0		
	6	31	36	−5	13	37	29	10		
	7	30	35	−4						
Average		32	31	1		42	34	30	36.0	36.8
SD		11	14	5		14	20	21		

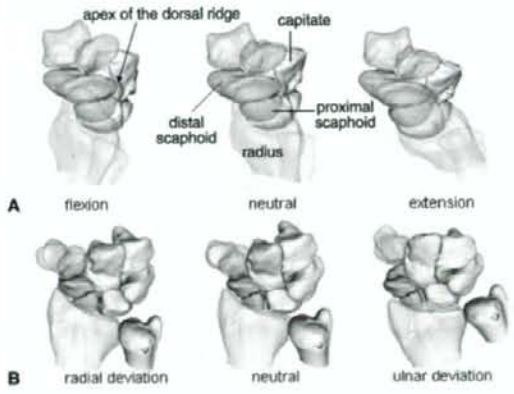

FIGURE 5: Motions of the stable type proximal pole nonunion (B3 type 1, case 10). The interfragmentary motions were small during both **A** the flexion-extension motion and **B** the radioulnar deviation. The proximal scaphoid is fixed, and the other bones are moving (these videos can be viewed at the *Journal's* Web site, www.jhandsurg.org).

and offer additional stability. This explains why the distal or volar type of nonunion is consistently associated with a DISI type of carpal malalignment.

In the current *in vivo* motion analysis, there were clearly 2 patterns of interfragmentary motions based on the fracture location. When the fracture was located distal to the scaphoid apex, the distal scaphoid was unstable relative to the proximal scaphoid (mobile type). The distal fragment showed a "book-opening" motion during motion from wrist flexion to extension. In contrast, when the fracture was located proximal to the apex, the amount of interfragmentary motion was significantly less than with the mobile type nonunion (stable type). In the mobile type, there was an uncoupling of the proximal and distal fragments, resulting in both abnormal kinematics and load distribution. Furthermore, the animations in the mobile type showed that the intercalated segment is no longer synchronized with the distal row by way of the scaphoid; the distal scaphoid fragment functionally becomes part of the distal row, and the proximal

scaphoid fragment is incorporated within the proximal row.

In patients with the B1 fracture (distal oblique fracture) and the B3 fracture (proximal pole fracture), there was a spectrum of fracture location as the fracture line runs close to the scaphoid apex. Regarding the B3 fracture, Garcia-Elias et al.[13] classified the proximal pole nonunion into type 1, where the fracture line runs proximal to the dorsal scapholunate interosseous ligament, and type 2, where the fracture line runs distal to the dorsal scapholunate interosseous ligament (Fig. 2). We confirmed that the kinematic patterns of type 1 and type 2 proximal pole nonunions were different; type 2 proximal pole nonunions were unstable and behaved identically to scaphoid waist nonunion (Fig. 4). Therefore, the natural history of type 2 nonunions should be different from that of type 1. In type 2, even though the fracture is located at the proximal pole, the bone defect is relatively large, and the patient will develop a DISI deformity and carpal instability. The proximal fragment usually has a capsular attachment at its dorsal aspect and a strong ligamentous connection with the lunate, which thus maintains some blood supply. Type 1 fractures essentially do not alter the equilibrium of forces between the scaphoid and the lunate. Because wrist stability is not at risk, the bone defect should be smaller, and the patient should have fewer symptoms. However, necrosis of the proximal fragment can easily occur due to the poor vascularity.

We classified B1 fractures (distal oblique fracture) into type 1, where the fracture line runs proximal to the scaphoid apex, and type 2, where the fracture line runs distal to the scaphoid apex (Fig. 2). The similar kinematic pattern as the proximal pole nonunion between type 1 and type 2 was found in the B1 oblique nonunions. We consider that the natural history of B1 type 2 nonunion should be different from B1 type 1 nonunion. However, further investigation is required to ascertain this theory because sample size in this study was indeed small.

Analysis for the rotation contribution rates revealed that there was a relative decrease in the motion between the radius and proximal scaphoid and the radiolunate motion in scaphoid nonunion when compared to the normal wrists. When a comparison was made between the mobile type and the stable type, however, there was no significant difference in contributions of the proximal scaphoid and the lunate. These results suggest that even stable scaphoid nonunion considerably affects radiocarpal kinematics. In contrast, the function of the midcarpal joint was relatively well preserved. This may explain why degenerative change following scaphoid nonunion starts from the radiocarpal joint.

There was no significant relationship between the interfragmentary motion and the duration (number of months) of the nonunion in this study. However, we can assume that the mobile nonunion would deteriorate more rapidly than the stable type nonunion and that the stable type nonunion would have a more chronic nature. We believe that the reason our results did not show a significant difference was due to the small number of the patients. On the other hand, it has been reported that a longstanding proximal third scaphoid nonunion can change the shape of the proximal fragment and develop a DISI deformity and severe degenerative changes.[14] Therefore, we also speculate that a longstanding nonunion of the stable type nonunion and resultant arthritis would change the kinematics within the scaphoid.

There is room for argument on other factors that may influence the stability on scaphoid nonunions, such as the mechanism of injury and the anatomic variance of the dorsal intercarpal ligament, which is controversial with respect to its insertion.[15] Moreover, Haase et al. reported that type 2 lunate morphology was associated with significantly decreased incidence of DISI deformity.[5] They theorized that the type 2 lunate's added articulation with the hamate lends some additional stability that resists abnormal extension of the lunate. They also found there was no association between lunate morphology and fracture location (proximal pole or waist). However, they did not classify their waist scaphoid fractures into subtypes, and it seems that their waist fracture group includes both Herbert B1 (distal oblique fracture) and B2 (waist fracture). It is possible that more exact classification of fracture location would clarify a more detailed relationship between lunate morphology, fracture location, and instability.

We found that the pattern of abnormal kinematics that occurs following scaphoid nonunion depends predominantly on whether the dorsal portion of the fracture line passes distal or proximal to the scaphoid apex. This study suggests that to identify the exact location of the fracture using 3-dimensional imaging is helpful in planning surgical tactics for the treatment of scaphoid nonunions. We hope this study raises concern regarding the scaphoid apex as a critical anatomic point in scaphoid nonunion pathology.

REFERENCES

1. Patterson RM, Moritomo H, Yamaguchi S, Viegas SF. Scaphoid anatomy and mechanics: update and review. Atlas Hand Clin 2004; 9:129–140.
2. Nakamura R, Imaeda T, Horii E, Miura T, Hayakawa N. Analysis of

scaphoid fracture displacement by three-dimensional computed tomography. J Hand Surg 1991;16A:485–492.
3. Moritomo H, Viegas SF, Elder KW, Nakamura K, DaSilva MF, Boyd NL, et al. Scaphoid nonunions: A 3-dimensional analysis of patterns of deformity. J Hand Surg 2000;25A:520–528.
4. Oka K, Moritomo H, Murase T, Goto A, Sugamoto K, Yoshikawa H. Patterns of carpal deformity in scaphoid nonunion: a 3-dimensional and quantitative analysis. J Hand Surg 2005;30A:1136–1144.
5. Haase SC, Berger RA, Shin AY. Association between lunate morphology and carpal collapse patterns in scaphoid nonunions. J Hand Surg 2007;32A:1009–1012.
6. Smith DK, Cooney WP III, An KN, Linscheid RL, Chao EYS. The effects of simulated unstable scaphoid fracture on carpal motion. J Hand Surg 1989;14A: 283–291.
7. Goto A, Moritomo H, Murase T, Oka K, Sugamoto K, Arimura T, et al. In vivo three-dimensional wrist motion analysis using magnetic resonance imaging and volume-based registration. J Orthop Res 2005;23:750–756.
8. Neu CP, Crisco JJ, Wolfe SW. In vivo kinematic behavior of the radio-capitate joint during wrist flexion-extension and radio-ulnar deviation. J Biomech 2001;34:1429–1438.
9. Moritomo H, Murase T, Goto A, Oka K, Sugamoto K, Yoshikawa H. In vivo, 3-dimensional kinematics of the midcarpal joint of the wrist. J Bone Joint Surg 2006;88A:611–621.
10. Crisco JJ, Coburn JC, Moore DC, Akelman E, Weiss AP, Wolfe SW. In vivo radiocarpal kinematics and the dart thrower's motion. J Bone Joint Surg 2005;87A:2729–2740.
11. Viegas SF, Patterson RM, Hillman GR, Peterson PD, Crossley M, Foster R. Simulated scaphoid proximal pole fracture. J Hand Surg 1991;16A:495–500.
12. Herbert TJ, Fisher WE. Management of the fractured scaphoid using a new bone screw. J Bone Joint Surg 1984;66B:114–123.
13. Garcia-Elias M, Lluch A. Partial excision of scaphoid: is it ever indicated? Hand Clin 2001;17:687–695.
14. Moritomo H, Tada K, Yoshida T, Masatomi T. The relationship between the site of nonunion of the scaphoid and scaphoid nonunion advanced collapse (SNAC). J Bone Joint Surg 1999;81B: 871–876.
15. Viegas SF, Yamaguchi S, Boyd NL, Patterson RM. The dorsal ligaments of the wrist: anatomy, mechanical properties, and function. J Hand Surg 1999;24A:456–468.

SCIENTIFIC ARTICLE

Change in the Length of the Ulnocarpal Ligaments During Radiocarpal Motion: Possible Impact on Triangular Fibrocartilage Complex Foveal Tears

Hisao Moritomo, MD, PhD, Tsuyoshi Murase, MD, PhD, Sayuri Arimitsu, MD, Kunihiro Oka, MD, PhD, Hideki Yoshikawa, MD, PhD, Kazuomi Sugamoto, MD, PhD

Purpose The fovea of the ulnar head is the primary attachment site for both the distal radioulnar and the ulnocarpal ligaments. Thus, both ligaments should be simultaneously affected by the traumatic avulsion of the triangular fibrocartilage complex from its ulnar attachment. Little attention, however, has been directed toward the role of the ulnocarpal ligaments in the mechanics of this type of injury. The purpose of this study was to investigate the changes in length of the ulnocarpal ligaments during various radiocarpal motions and to determine the type of radiocarpal motion that makes the ulnocarpal ligament taut and that could cause foveal avulsion if it were excessive.

Methods The 3-dimensional kinematics of the wrist joint were investigated noninvasively using a markerless bone registration technique *in vivo*. Magnetic resonance images of the wrists of 15 healthy volunteers were acquired in at least 5 positions during each wrist flexion–extension motion, radioulnar deviation, or the so called dart-throwing motion (radial extension–ulnar flexion motion). The 3-dimensional ligament paths of the ulnotriquetral, ulnolunate, ulnocapitate, and palmar radioulnar ligaments were modeled as the shortest paths between the fovea and the insertion point of each ligament. Changes in the 3-dimensional ligament length of each ligament between the neutral position and each wrist position were then calculated.

Results The lengths of the ulnotriquetral and ulnocapitate ligaments increased the most on wrist radial extension, and the length of the ulnolunate ligament increased the most on wrist extension. The length of the palmar radioulnar ligament changed minimally during any motion.

Conclusions The ulnocarpal ligaments are likely to be stretched tensely in wrist radial extension and wrist extension. This study supports the hypothesis that one of the mechanisms responsible for a triangular fibrocartilage complex foveal tear is excessive traction of the ulnocarpal ligament caused by a fall on the outstretched hand. *(J Hand Surg 2008;33A:1278–1286. Copyright © 2008 by the American Society for Surgery of the Hand. All rights reserved.)*

Key words Biomechanics, fovea, triangular fibrocartilage complex, ulnocarpal ligament, wrist.

Additional material is available online.

From the Department of Orthopaedics, Osaka University Graduate School of Medicine, Osaka, Japan.

Received for publication August 7, 2007; accepted in revised form April 30, 2008.

Supported in part by Grants-in-aid for Scientific Research, the Ministry of Education, Science, and Culture of Japan.

Corresponding author: Hisao Moritomo, MD, PhD, Department of Orthopaedics, Osaka University Graduate School of Medicine. 2-2 Yamadaoka, Suita-shi, Osaka, 565-0871, Japan; e-mail: moritomo@ort.med.osaka-u.ac.jp.

0363-5023/08/33A08-0003$34.00/0
doi:10.1016/j.jhsa.2008.04.033